Crosslinkable TAPC-Based Hole-Transport Materials for Solution-Processed Organic Light-Emitting Diodes with Reduced Efficiency Roll-Off

*Georgios Liaptsis and Klaus Meerholz**

1-Bis[4-[*N*,*N*-di(4-tolyl)amino]phenyl]-cyclohexane (TAPC) has been widely used in xerography and organic light-emitting diodes (OLEDs), but derivatives are little known. Here, a new series of solution-processable, crosslinkable hole conductors based on TAPC with varying highest occupied molecular orbital (HOMO) energies from –5.23 eV to –5.69 eV is implemented in blue phosphorescent OLEDs. Their superior perfomance compared with the well-known N4,N4,N4′,N4′-tetraphenylbiphenyl-4,4′-diamine (TPDs) analogues regarding hole-injection and mobility, electron and exciton blocking capabilities, efficiency, and efficiency roll-off is demonstrated. Overall, the TAPC-based devices feature higher luminous and power efficiency over a broader range of brightness levels and reduced efficiency roll off. A systematic broadening of the emission zone is observed as the hole-injection barrier between the anode and the hole-transporting layer increased.

1. Introduction

Organic light-emitting diodes (OLEDs) are of strong interest for display and solid-state lighting applications owing to their low power consumption, wide viewing angle and low production costs.[1,2] They consist of one or more organic layer(s) sandwiched between a transparent indium-tin-oxide (ITO) anode and a reflective metal cathode (back contact). For improved device characteristics, like the luminous efficiency, efficiency roll-off and high brightness, a multi-layer design is favorable over single-layer OLEDs.[3] In vacuum-processed devices, this is straight forward. In order to realize a multi-layer OLED processed from solution, it is necessary to form insoluble films before depositing the subsequent layers. In the past, we have introduced oxetane moieties to small-molecule precursors, allowing crosslinking of the materials through photoinitiated cationic ring-opening polymerization (CROP) without impeding their electrooptic properties.[4] Subsequently, additional layers can be deposited.[4,5]

The focus of our and others[6] work has been on hole conductors based on tetraphenylene-benzidine, -phenylene, -fluorene[4,7,8] derivatives as well as conjugated[5] or non-conjugated[9] arylamine containing polymers in organic electronics aiming improved hole-transport as well as hole-injection into the emissive organic material of OLEDs using low cost fabrication techniques.

In this study, we introduce a new series of crosslinkable hole-conducting materials based on 1-bis[4-[*N*,*N*-di(4-tolyl)amino]phenyl]-cyclohexane (XTAPC), which is well known for its high hole mobility and high triplet energy[10,11] and has been widely used as hole injection layer for OLEDs[12] or xerographic applications.[13] Due to their smaller conjugated system, TAPCs generally feature a larger bandgap compared to TPD-type compounds (e.g., the commonly used aNPD). Thus, for similar HOMO (highest occupied molecular orbital) levels, higher LUMO (lowest unoccupied molecular orbital) energies are expected, promising improved electron-blocking capabilities. Further, due to the enhanced triplet energy of TAPC compared to TPD evaporated small-molecule OLEDs based on TAPC using FIrpic as dopand showed better device performance than the TPD analogues.[14] We will show that the HOMO of the TAPC based compounds can be varied by introducing electronically withdrawing or donating groups to the aromatic core. We investigate the use of the TAPCs in blue-emitting, phosphorescent OLEDs (PHOLEDs). Compared with the XTPDs, XTAPCs generally show greatly improved performance. In addition, a systematic shift of the emission color is observed when the injection barrier between the poly(3,4-ethylenedioxythiophene):poly(styrenesulfonate) (PEDOT:PSS) anode and the adjacent hole conductor varies, indicative of a change of the width of the emission zone (EMZ) inside the device. This is confirmed by numerical simulations. Overall, the TAPC-based devices feature higher luminous and power efficiency over a broader range of brightness levels.

G. Liaptsis, Prof. K. Meerholz
Physikalische Chemie
Universität zu Köln
Luxemburger Straße 116, 50939 Köln, Germany
E-mail: klaus.meerholz@uni-koeln.de

DOI: 10.1002/adfm.201201197

2. Results and Discussion

2.1. Synthesis, Electrochemical and Photophysical Properties

Crosslinkable hole-transport materials (XHTMs) based on the TAPC motif were synthesized by subsequent Pd(0)-catalyzed

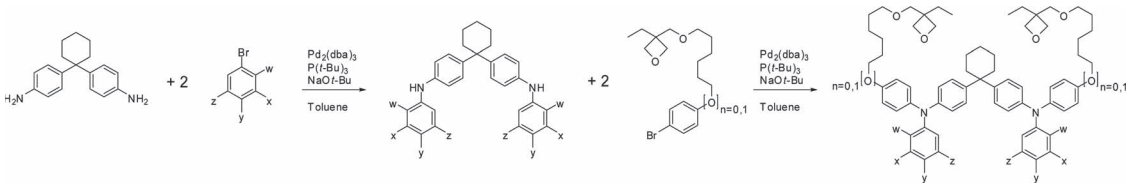

Scheme 1. General reaction scheme for the synthesis of X-TAPCs using subsequent Buchwald-Hartwig amination reactions.

Buchwald-Hartwig cross-coupling reactions[15,16] between 4,4′-(cyclohexane-1,1-diyl)dianiline and the corresponding bromoarene under basic conditions (**Scheme 1**) in acceptable to good overall yields (**Table 1**). Firstly, different bromoarenes (varying in the respective substituents w through z; Table 1) were coupled to the corresponding dianiline. Secondly, hexylether- and oxetane-group-containing bromoarenes were coupled with the bis-diphenylamine to the final products. The side chain increases the solubility, and the oxetane units can be reacted via cationic ring-opening polymerization (CROP) to crosslink the films after deposition for subsequent multi-layer fabrication. The chemical structures of the TAPCs are shown in Figure S1 (Supporting Information). All compounds were fully characterized by ^{1}H-NMR, ^{13}C-APT NMR, high resolution ESI-MS spectroscopy, and elementary analysis. The new compounds **X-TAPC 4** is most closely related to the parent compound **TAPC** itself (tetra-alkyl substitution; see Figure S1, Supporting Information).

The electrochemical properties of the new compounds were investigated by cyclic voltammetry in dichloromethane with tetrabutylammonium hexafluorophosphate as supporting electrolyte and ferrocene/ferrocenium as internal standard. All compounds exhibit two reversible oxidation steps. Using the expression (1), the oxidation potentials can be converted into the HOMO energies versus vacuum level (Table 1):

$$E_i = (5.1 \pm 0.05)\text{eV} + E_{ox}(0.9 \pm 0.1)\text{eV V}^{-1} \quad (1)$$

where –5.1 eV is the HOMO energy of ferrocene, and 0.9 is a solvent-dependent correction factor.[17]

UV/Vis absorption spectra were recorded in dichloromethane to obtain the transition energy from ground state (S_0) to the first excited state (S_1). A multi-Gaussian fit was used to model the absorption spectra, and the maximum of the most bathochromic Gaussian curve was assigned to the transition energy $S_0 \Rightarrow S_1$. All new HTMs show a main absorption band around 4 eV. The X-TAPCs **7** and **9** featuring trifluoro-methyl substituents show a second, smaller and bathochromically shifted absorption around 3.5 eV. The energy level of the LUMO was estimated by adding the transition energy to the HOMO level (Table 1). Additionally, low-temperature photoluminescence (PL) spectra of films of most of the novel **X-TAPCs** were recorded at 80 K to obtain their triplet energies. Therefore, the PL intensity was integrated for 5 ms 300 µs after the excitation pulse. For all measured compounds a triplet level of 2.87 eV was observed from the onset of photoluminescence (Figure S3,

Table 1. Synthesis, yield and electronic properties. Overall yield of the new X-TAPCs depending on the different substituents (w, x, y, z) on their aromatic core (see Figure 1). First and second oxidation potential measured by cyclic voltammetry calibrated vs. the ferrocene/ferrocenium redox couple, wavelength of maximum absorption, and calculated HOMO and LUMO energies.

X-TAPC	n	w	x	y	z	Yield	E_{Ox1}	E_{Ox2}	λ_{max}	E_{HOMO}	E_{LUMO}	μ_{SCLC}
						[%]	[V]	[V]	[nm]	[eV]	[eV]	[cm^2 V s^{-1}]
1	1	H	H	OMe	H	66	0.140	0.220	306	–5.23	–1.22	1.17×10^{-6}
2	0	H	H	OMe	H	66	0.220	0.305	306	–5.30	–1.31	1.98×10^{-7}
3	1	H	H	F	H	45	0.290	0.355	303	–5.36	–1.31	2.06×10^{-8}
4	0	H	H	Me	H	44	0.295	0.390	309	–5.37	–1.39	5.20×10^{-8}
5	0	H	H	F	H	53	0.390	0.470	303	–5.45	–1.41	5.21×10^{-8}
6	1	H	F	F	F	64	0.465	0.520	296	–5.52	–1.47	4.35×10^{-9}
7	1	CF_3	H	CF_3	H	32	0.515	0.580	294, 350 (sh)[a)]	–5.56	–2.12	2.45×10^{-9}
8	0	H	F	F	F	70	0.590	0.665	300	–5.63	–1.63	1.53×10^{-8}
9	0	CF_3	H	CF_3	H	62	0.650	0.745	296, 347 (sh)[a)]	–5.69	–2.19	1.23×10^{-9}
XF6TPD[b)]							0.460	0.640	346	–5.51	–2.17	1.42×10^{-9}
PVK[b)]										–5.90	–2.20	
FIrpic[b)]										–5.89	–3.10	
OXD-7[b)]										–6.30	–2.40	

[a)] (sh) shoulder; [b)] HOMO and LUMO energies have been taken from ref. [14].

Supporting Information), which is much higher than the triplet energy of TPDs (2.34 eV).[14] Note that delayed fluorescence is convoluted in the spectra of **X-TAPC 4**. The high triplet state of the **X- TAPC** prevents energy back transfer from the triplet level of FIrpic (2.7 eV) to the adjacent hole transport layer.

2.2. Single-Carrier Devices

The single-carrier devices consisting of the corresponding X-TAPC layer sandwiched between an ITO/PEDOT anode and a non-injecting gold cathode were investigated. Assuming an ohmic contact between the injecting electrode and the active material and trap-free volume transport, the current-voltage (J–V) characteristics can be described by the Mott-Gurney Law:

$$J_{SCLC} = \frac{9}{8}\mu_h \varepsilon_0 \varepsilon_r \frac{V^2}{d^3} \quad (2)$$

Here, μ_h is the hole mobility, V the applied voltage, d the active layer thickness, and ε_0 and ε_r are the permittivity of free space and the relative permittivity of the material (which is set to 3 in the following calculations), respectively.

Hole-mobilities were determined by fitting the SCLC regime of the J–V curves using Equation 2. Formally, the assumption of an ohmic contact is fulfilled for compounds **1** to **4** only (injection barrier between PEDOT:PSS and HOMO of the corresponding X-TAPC < 0.3 eV), but due to the rather low mobilities μ_{SCLC} featured by the other compounds (Table 1), the SCLC conditions are maintained for all compounds despite of the large injection barriers.[18] There seems to be a rough correlation between μ_{SCLC} and the molecular polarity, resulting from the alkoxy- (donor) and fluorine-, trifluoro-methyl (acceptor) substitution on the TAPC aromatic core. Compared to **XF6TPD**, the TPD-type hole conductor, which gave the best PHOLED performance in previous experiments all X-TAPCs show an improved or similar hole-mobility.

2.3. Single-HTL OLEDs

In our previous work, we introduced different hole-transport layers based on crosslinkable TPDs (X-TPDs) between PEDOT:PSS and the emitter layer in blue-phosphorescent OLEDs (PHOLEDs), in which the emitting layer (EML) consisted of PVK/OXD–7/FIrpic (68/27/5 wt%; see **Figure 1** for chemical structures).[17] We demonstrated that the maximum luminous efficiency correlated with the HOMO energy of the HTL, the best performance was achieved, when the hole-injection barrier between PEDOT:PSS and the PVK matrix was divided into two equal steps. However, the electron blocking properties of the TPDs, which also varied within this series, were not considered.

To examine the new crosslinkable, large-bandgap X-TAPCs in terms of their device performance we fabricated similar blue PHOLEDs. The device configuration was as follows: a 35 nm thin layer PEDOT:PSS was spincast on ITO-coated glass followed by deposition of a 10 nm thin layer of a X-TAPC. After crosslinking of the HTL, the EML was spin-cast on top in a thickness of 80 nm.[17,19–20] Finally, the cathode (4 nm CsF and 100 nm Al) was deposited via thermal evaporation.[21,22]

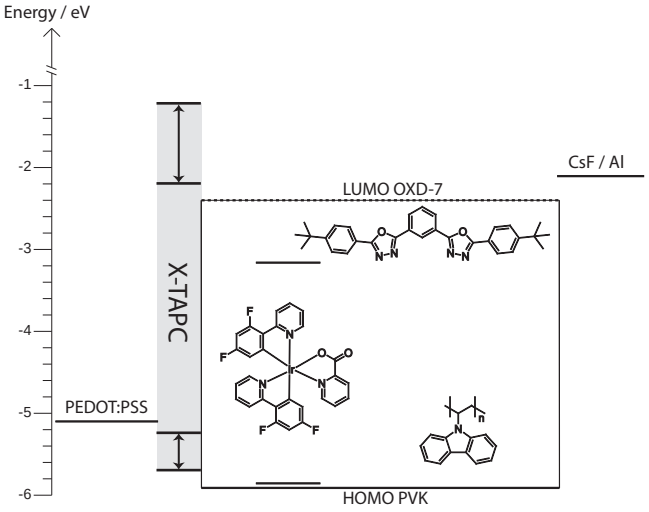

Figure 1. Energy level diagram for compounds used in blue PHOLEDs. HOMO and LUMO energies for Firpic are shown in black bars. PVK HOMO energy is shown as black line and OXD-7 LUMO energy is shown as dotted line. Inset: chemical structures of the compounds used in the EML.

In **Figure 2**, the maximum luminous efficiency of the PHOLEDs containing a single X-TAPC layer is plotted as a function of their HOMO energy. The device efficiency increases from 13.7 Cd A^{-1} for **1** (HOMO energy –5.23 eV) to >18 Cd A^{-1} for **4–8** and decreases again to 15.7 Cd A^{-1} for **9** (–5.69 eV). For comparison we also included data of our previous work on X-TPDs. Obviously, compared to X-TPDs with similar HOMO levels the device performance is significantly improved by up to a factor of 2 for compounds **1** and **9**, featuring the highest or lowest HOMO level, respectively. We attribute this to the enhanced electron/exciton blocking ability of the TAPCs at the HTL/EML interface.

For both device series, X-TPDs and X-TAPCs, the maximum luminous efficiency is obtained when the hole-injection barrier between PEDOT:PSS (–5.1 eV) and PVK (–5.9 eV) is divided into two almost identical steps (i. e. when HOMO is at ca. –5.5 eV), reaching slightly higher efficiencies (up to 18.5 Cd A^{-1}) compared with the reference device without HTL (**REF**: 18.1 Cd A^{-1}). However, while the maximum luminous efficiency clearly peaks for the TPD-series, it is less distinct for the X-TAPCs. Please note, that devices based on **3**, **6** and **7** featuring a donor and acceptor substitution pattern on the aromatic units do not follow the trend of the other compounds. This might be explained by an increased permanent dipole moment of these molecules, resulting in a decreased hole-mobility (compare Section 2.2).[23,24] Such compounds were not investigated in our previous study on TPDs.

Table 2 summarizes the performance of the full device series and compares the results with those obtained for devices without a HTL (**REF**) or with the best TPD derivative (**XF6TPD**). Compared to the **REF** device, all other devices feature reduced onset voltages despite the fact that the total layer thickness is increased by 10 nm (one HTL) or even 20 nm (double HTL). The lowest onset voltage is achieved using X-TAPC **1**. The

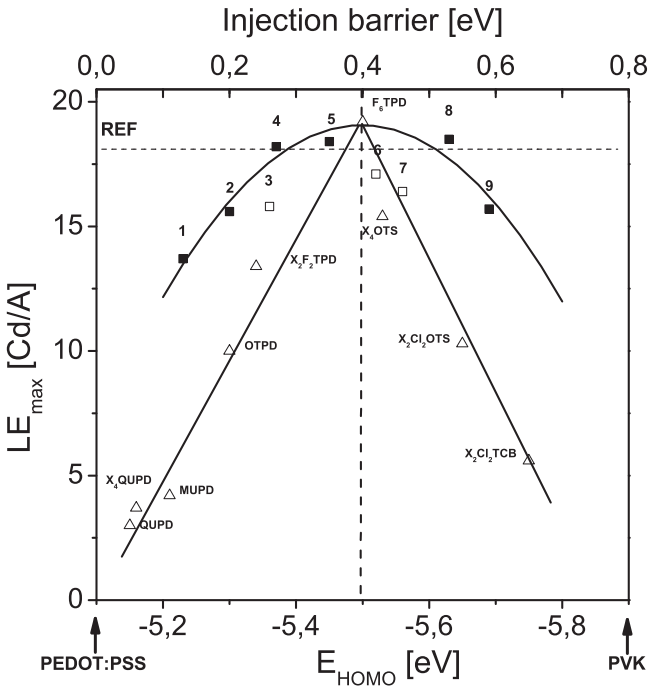

Figure 2. Maximum luminous efficiency of blue PHOLEDs with single-layer XTAPCs **1–9** (filled and open squares). The maximum luminous efficiency of the reference device (**REF**) without HTL is shown as dashed line. Data obtained using X-TPDs are included for comparison (open up triangles).[11] The bottom axis shows the HOMO energy of the respective compound (Table 1); the energy levels of the injection layer PEDOT:PSS and of PVK, the matrix material used in the EML are indicated by arrows. The top axis shows the injection barrier between PEDOT:PSS and the XHTL assuming energy level alignment. The solid lines are guide to the eye. The vertical dashed line indicates the case, when the injection barrier is subdivided into two identical steps.

device starts to emit (EL > 0.1 Cd/A) at an applied voltage of 2.85 V. Within the X-TAPC series the onset voltage increases up to 4.50 V using X-TAPC **9**, which is still superior to the REF device (4.70 V). The maximum performance of devices containing XTAPC **4** and even more so the double-HTL device **2/5** exceed the performance of **REF**, demonstrating a superior performance within optimized HTL due to more facilitated hole-injection and increased electron blocking ability.

2.4. Color Shift

Within the entire device series, the CIE color coordinates of the emission shift from greenish blue for device using X-TAPC **1** as HTL (x = 0.194, y = 0.392)to a deeper blue for X-TAPC **9** (x = 0.172, y = 0.364; Table 2).

This might be attributed to a spatial variation of the emission zone (EMZ) within the EML, which is largely affected by the charge-carrier balance inside the EML. This balance is influenced by both, charge-injection and charge-transport properties of the layers.[25,26] By using the software Etfos 1.5 (Fluxim AG) the EMZ can be qualitatively derived from the electroluminescence (EL) spectra.[27,28] As input for the internal emission spectrum of the EML the normalized photoluminescence spectrum of an 80 nm film of the PVK/OXD-7/FIrpic blend was used.

From the best fit of the simulation to the experimental EL spectra (**Figure 3**a) at constant current densities of 1 mA cm^{-2}, the EMZs of the devices were obtained. The results for the device containing X-TAPCs **1**, **4**, **9** and the **REF** device are shown in Figure 3b. While the EMZ is narrow for compound **1**, its width increases approximately linearly (Figure 3c) when the injection barrier between PEODT and X-TAPC increases. Simultaneously, the height of the EMZ is reduced owing to a more extended hole distribution within the EML at comparable brightness's. This affects the outcoupling of discrete wavelengths resulting

Table 2. Device data for single-, double-, and no-HTL devices Maximum luminous efficiency LE_{max} and the corresponding voltage U, luminous efficiency at a brightness of 1000 Cd m^{-2} LE_{1000} and the corresponding voltage U, maximum power efficiency PE_{max} and the corresponding voltage U, onset voltage U_{on}, and CIE-values (x,y) measured at a current density of 1 mA cm^{-2}.

X-TAPC	LE_{max} [Cd A^{-1}]	U [V]	LE_{1000} [Cd A^{-1}]	U [V]	PE_{max} [lm W^{-1}]	U [V]	U_{on} [V] at 0.1 [Cd m^{-2}]	CIE	
								x	y
1	13.7	6.50	11.3	9.50	8.1	4.50	2.85	0.1939	0.3918
2	15.6	7.25	14.0	9.00	8.1	5.50	2.95	0.1811	0.3769
3	15.8	7.75	15.3	8.75	7.8	5.00	3.10	0.1712	0.3660
4	18.2	6.75	16.8	9.00	10.4	4.50	3.10	0.1761	0.3681
5	18.4	7.25	18.1	8.75	9.8	4.50	3.30	0.1702	0.3689
6	17.2	7.25	15.7	9.00	8.0	6.00	3.70	0.1676	0.3590
7	16.4	7.50	14.3	9.75	8.0	5.75	3.95	0.1712	0.3627
8	18.5	7.75	16.7	9.50	8.3	6.25	4.10	0.1711	0.3610
9	15.7	7.75	13.6	10.00	6.8	6.75	4.50	0.1731	0.3643
2/ 5	18.4	7.00	17.3	9.50	11.3	4.00	3.25	0.1729	0.3612
5/ 8	17.6	8.00	14.0	12.00	9.8	4.50	3.75	0.1723	0.3599
XF6TPD	19.1	7.25	16.3	9.50	9.1	6.00	4.10	0.1697	0.3578
REF	18.1	7.25	18.0	7.50	8.8	6.50	4.70	0.1652	0.3606

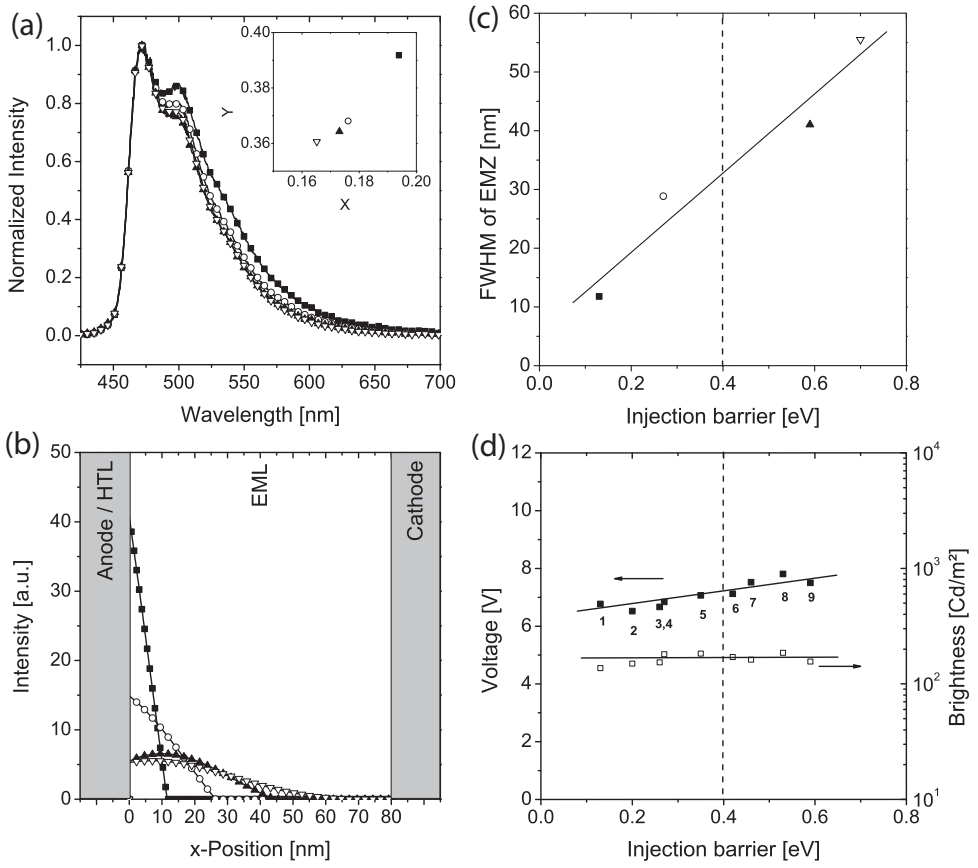

Figure 3. a) Normalized experimental EL spectra of the devices based on **1** (filled squares), **4** (open circles), **9** (filled up triangles), and **REF** device (open down triangles) measured at 1 mA cm^{-2}. The inset diagram shows the corresponding CIE x and y values (Table 2). b) Relative distribution of the EMZ in the OLEDs simulated from their corresponding EL-spectra (see subfigure a). c) Width (FWHM) of the emission zone (EMZ) for the above devices as a function of the injection barrier between PEDOT:PSS and the XHTL. The solid black line is a guide to the eye. d) Operating voltage (left axis and closed symbols) and brightness (right axis, open symbols) of devices operated at a current density of 1 mA/cm^2 as a function of the injection barrier. The solid lines are guide to the eye. The vertical dashed lines in (c,d) indicate in the case, when the injection barrier is divided into two identical steps.

in a color shift of the EL-spectra from greenish blue to deeper blue due to the variation of the X-TAPCs. In comparison, the **REF** device exhibits the broadest and least intense EMZ profile. Note, that the emission intensity is roughly constant for all devices when operated at 1 mA cm^{-2} (Figure 3d, open squares), indicating constant efficiency. The drive voltage increases slightly (by ca. 1 V) due to the variation of the hole-injection barrier (Figure 3d, closed squares).

In addition, we studied the changes of the emission for different drive voltages. While there is a significant broadening of the EMZ for devices based on **1** and **4**, this effect is almost vanished in **9** (Figure S2 (Supporting Information) and bars in Figure 3a). This is explained due to an increasing displacement of the holes towards the cathode when the electric field is increased. By contrast, the effect is reversed in the **REF** device, probably due to enhanced electron injection.

2.5. Double-HTL OLEDs and Comparison with TPDs

For further optimization, devices with a double-HTL structure were fabricated. In these cases, the maximum injection barrier for holes was identical (0.35 eV), while its position varies: it is next to the EML for **2**/**5** interlayers, or next to PEDOT:PSS for **5**/**8** interlayers. These double-HTL devices show also high efficiency (17.6 Cd A^{-1} at 8.00 V and 18.4 Cd A^{-1} at only 7.00 V despite its increased device thickness of 20 nm) and the highest power efficacy of 11.3 lm W^{-1} at 4.00 V for the **2**/**5** interlayers (**REF**: 8.8lm W^{-1} at 6.50 V, best single-HTL: 10.4 lm W^{-1} at 4.50 V) (**Figure 4**; Table 2) due to facilitated hole injection.

Until now, we have only compared the optimum performance (maximum values). Now, we will consider the full voltage range:

i) As already pointed out above, the maximum luminous efficiency [cd/A] is very similar in all devices and is observed at operating voltages of ca. 7–8 V. This indicates that the balance between holes and electrons is ideal under these conditions). By contrast, distinct differences are observed for lower and/or higher voltages, hinting that the hole/electron ratio becomes non-ideal. Fortunately, the introduction of the HTL significantly broadens the J–V curves compared to the **REF** device, which features a rather narrow maximum.

ii) The power efficacy [lm/W] is similar for U > 8 V, whereas larger differences are observed for U < 7 V. Again, introduction of the HTL improves the performance at all voltages compared to the REF device.

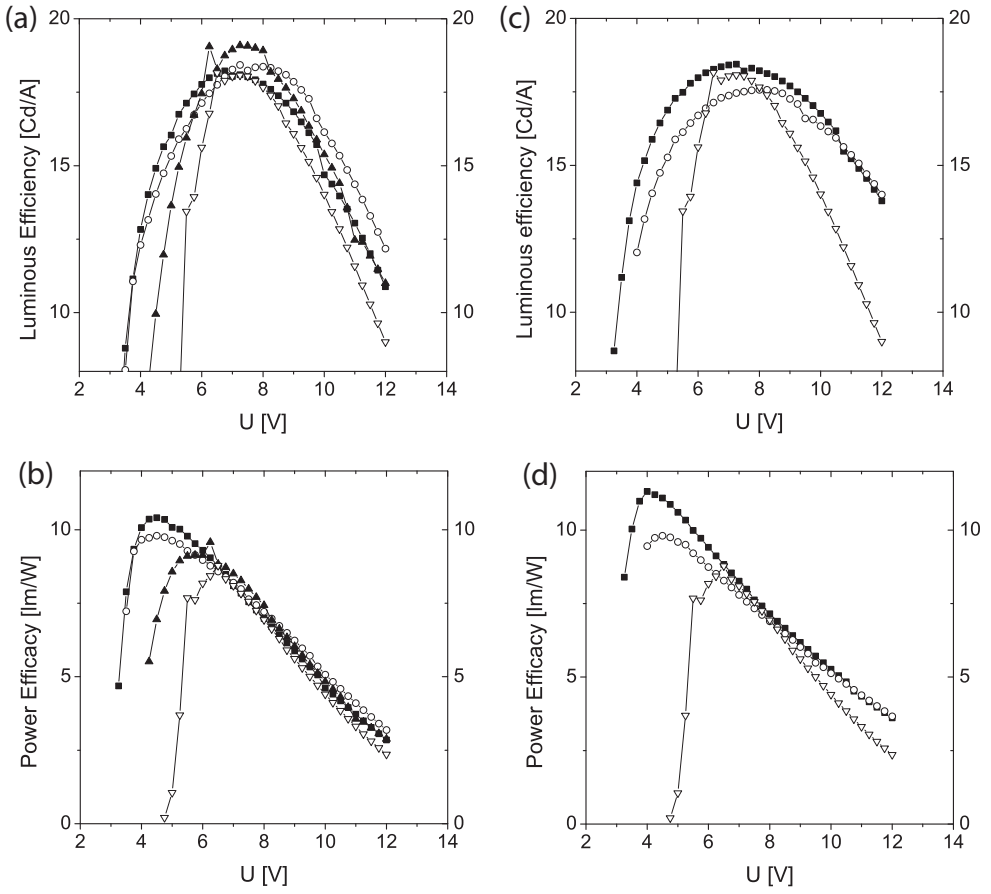

Figure 4. Luminous efficiency (a,c) and power efficacy (b,d) as a function of the operating voltage. a,b) Single-HTL devices based on **4** (E_{HOMO} = –5.37 eV; filled squares), **5** (E_{HOMO} = –5.45 eV; open circles), and **XF6TPD** (E_{HOMO} = –5.50 eV; open up triangles). c,d) Double-HTL devices based on **2**/**5** (E_{HOMO} = –5.30/E_{HOMO} = –5.45 eV; filled squares) and **5**/**8** (E_{HOMO} = –5.45 eV/E_{HOMO} = –5.63 eV; open circles). In both cases, the reference device **REF** without HTL is shown in open down triangles.

iii) Direct comparison of the performance of devices **5** and **XF6TPD**, which have similar HOMO energy (–5.51 eV and –5.45 eV, respectively; see Table 1) shows strongly improved performance for XTAPC **5** at low voltages (light levels below 100 Cd m^{-2}) as well as improved efficiency roll-off at high voltages (Figure 4). This finding is clear evidence for the better electron-blocking capabilities of **XTAPC-5** compared with **XF6TPD**, the barrier for electrons increases by ca. 0.7 eV (see Table 1).

iv) The best overall performance regarding both, power efficacy (>11 lm/W) and luminous efficiency (>18 Cd/A), as well as for the efficiency roll-off is obtained with the double-HTL device **2**/**5**, while the **REF** device is worst (Figure 4c,d; Table 2).

3. Conclusion

In conclusion, we have introduced a novel class of crosslinkable hole conductors based on the TAPC motif for multilayer OLED fabrication from solution. These compounds generally feature a larger bandgap and a higher triplet energy level than the commonly used TPD-type hole conductors. As a result, for compounds with similar HOMO level the electron and/or excition blocking capabilities of the TAPC derivatives are more favorable. We demonstrated the beneficial impact onto the performance of prototypical blue PHOLEDs. While the maximum luminous efficiency was essentially unchanged, the power efficiency and efficiency roll-off were improved due to the enhanced electron-blocking capabilities of the TAPCs as compared to TPDs. Using optical simulations, it was demonstrated for the first time that the EMZ broadens as the hole-injection barrier increases.

4. Experimental Section

Synthesis: All chemicals were used as received from commercial suppliers. Buchwald-Hartwig amination reactions were carried out under argon atmosphere in degassed and dry toluene. A mixture of corresponding dianiline and appropriate equivalents of bromoarene using 1 mole percent of $Pd_2(dba)_3$, 1.6 mole percent of $P(tBu)_3$ and 1.5 equivalents of NaO*t*Bu per reacting N*H* were heated for 2 to 24 h at temperatures between 40 and 80 °C. Completion of the reactions was monitored by TLC and ESI-MS, if so, the reaction was diluted with EtOAc, washed with water, re-extracted with EtOAc and dried over $MgSO_4$. After evaporation of the solvent, the desired product was purified by mid-pressure liquid chromatography (MPLC) eluting with toluene/ethylacetate mixtures at a constant flow of 20 mL/min.

Nuclear Magnetic Resonance Spectroscopy: The ^{1}H-NMR or ^{13}C-NMR spectra were recorded on a Bruker DPX 300 spectrometer using chloroform-d_1 as the solvent.

High Resolution ESI-MS: The high resolution ESI-MS spectra were recorded on a Thermo Scientific LTQ Orbitrap XL.

Elementary Analysis: The elementary analysis was performed on a Euro EA 3000 (CHNS), HEKAtech.

Electrochemical Measurements: Cyclic voltammetry was performed with an EG&G Instruments Potentiostat/Galvanostat Model 283 in 10^{-3} molar solutions of appropriate HTM in dry dichlormethane with 0.1 M tetrabutylammonium hexafluorophosphate as supporting electrolyte. Platinum wires were used for working and counter electrodes whereas a silver wire was used for reference electrode. All measurements were carried out at room temperature without inert gas atmosphere and were correlated to the ferrocenium/ferrocene redox couple as internal standard.

UV/VIS absorption spectroscopy: UV/VIS absorption spectra were recorded with a CARY 50, VARIAN spectrometer from 10^{-5} molar dichlormethane solution in a 10 mm diameter quartz cuvette.

Fluorescence Spectroscopy: Fluorescence spectra from a 80 nm thin spincast film was recorded with a CARY ECLIPSE VARIAN spectrometer.

Low Temperature Photoluminescence Spectroscopy: The compounds were excited with the third harmonic (355nm) of a Nd:YAG (Spitlight, Innolas). The laser operated at a repetition rate of 10 Hz. The PL was collected and focused onto the entrance slit of the monochromator and detected by an intensified gateable ICCD camera (Roper Scientific).

Single-Carrier Devices: Single carrier devices were fabricated on ITO-coated glass substrates which were thoroughly cleaned and treated with ozone plasma. A layer of PEDOT:PSS (Baytron P, AI4083, Heraeus Clevios) was spincast onto the substrates and backed at 120°C for 120 s. The substrates were transferred to a nitrogen filled glove-box where the crosslinkable HTMs were spincast from 20.0 mg mL^{-1} toluene solutions containing 1.51 wt% 4-octyloxydiphenyliodonium hexafluoroantimonate (OPPI) as photoinitiator. The films were irradiated with UV light (310 nm) for 10 s and backed at 110 °C to promote crosslinking yielding a 100 nm thick film. The spin coating and crosslinking procedure was done twice to yield a layer thickness of 200 nm.

OLED Fabrication and Measurement: The OLEDs were fabricated on ITO-coated glass substrates which were thoroughly cleaned and treated with ozone plasma. A layer of PEDOT:PSS (Baytron P, AI4083, Heraeus Clevios) was spincast onto the substrates and backed at 120 °C for 120 s. The substrates were transferred to a nitrogen filled glove-box where the crosslinkable HTMs were spincast from 3.0 mg mL^{-1} toluene solutions containing 4 mol% 4-octyloxydiphenyliodonium hexafluoroantimonate (OPPI) as photoinitiator. The films were irradiated with UV light (310 nm) for 10 s and backed at 110 °C to promote crosslinking. Afterwards the emitting blend consisting of PVK, OXD-7 (28 wt%) and FIrpic (5 wt%) in chlorobenzene (15 mg mL^{-1}) was spincast on top. Subsequently, the cathode was deposited by thermal evaporation at 10^{-9} bar. The current-voltage-luminescence characteristics were measured with an Keithley 2400 amperometer and a calibrated photodiode.

Simulation: For optical simulation the software Etfos 1.5 (Fluxim AG) which uses the transfer-matrix formalism was used. As internal spectra for simulations a normalized photoluminescence spectrum of a 80 nm film on glass of the emitting blend consisting of PVK, OXD-7 (28 wt%) and FIrpic (5 wt%) spincast from chlorobenzene (15 mg mL^{-1}) was used. The thickness of the different layers were set as follows: 100 nm Alumina-cathode, 80 nm EML, 10 nm HTL, 35 nm PEDOT:PSS, 130 nm ITO.

Supporting Information

Supporting Information is available from the Wiley Online Library or from the author.

Acknowledgements

The authors thank Dr. Dirk Hertel for experimental help within low temperature photoluminescence spectroscopy. Further, they thank Dr. Dirk Hertel and Dr. Ronald Alle for fruitful discussions. Aditionally, the authors thank Radouane Nagim for the HR-ESI-MS measurements and Silke Kremer for the EA measurement. All persons mentioned above are with the University of Cologne.

Received: May 1, 2012
Revised: July 10, 2012
Published online: August 28, 2012

[1] R. H. Friend, R. W. Gymer, A. B. Holmes, J. H. Burroughes, R. N. Marks, C. Taliani, D. D. C. Bradley, D. A. Dos Santos, J. L. Bredas, M. Logdlund, W. R. Salaneck, *Nature* **1999**, *397*, 121.
[2] C. D. Muller, A. Falcou, N. Reckefuss, M. Rojahn, V. Wiederhirn, P. Rudati, H. Frohne, O. Nuyken, H. Becker, K. Meerholz, *Nature* **2003**, *421*, 829.
[3] S. Reineke, F. Lindner, G. Schwartz, N. Seidler, K. Walzer, B. Lussem, K. Leo, *Nature* **2009**, *459*, 234.
[4] M. S. Bayerl, T. Braig, O. Nuyken, D. C. Muller, M. Gross, K. Meerholz, *Macromol. Rapid Commun.* **1999**, *20*, 224.
[5] S. Jungermann, N. Riegel, D. Muller, K. Meerholz, O. Nuyken, *Macromolecules* **2006**, *39*, 8911.
[6] F. Huang, Y. J. Cheng, Y. Zhang, M. S. Liu, A. K. Y. Jen, *J. Mater. Chem.* **2008**, *18*, 4495.
[7] X. H. Yang, D. C. Muller, D. Neher, K. Meerholz, *Adv. Mater.* **2006**, *18*, 948.
[8] D. C. Muller, T. Braig, H. G. Nothofer, M. Arnoldi, M. Gross, U. Scherf, O. Nuyken, K. Meerholz, *ChemPhysChem* **2000**, *1*, 207.
[9] J. Schelter, G. F. Mielke, A. Kohnen, J. Wies, S. Kober, O. Nuyken, K. Meerholz, *Macromol. Rapid Commun.* **2010**, *31*, 1560.
[10] P. M. Borsenberger, L. Pautmeier, R. Richert, H. Bassler, *J. Chem. Phys.* **1991**, *94*, 8276.
[11] K. Goushi, R. Kwong, J. J. Brown, H. Sasabe, C. Adachi, *J. Appl. Phys.* **2004**, *95*, 7798.
[12] C. W. Tang, S. A. Vanslyke, *Appl. Phys. Lett.* **1987**, *51*, 913.
[13] P. M. Borsenberger, D. S. Weiss, *Organic Photoreceptors for Xerography*, 59 Optical Engineering Series, Marcel Dekker Inc, **1998**.
[14] J. Lee, N. Chopra, S. H. Eom, Y. Zheng, J. G. Xue, F. So, J. M. Shi, *Appl Phys Lett* **2008**, *93*, 123306.
[15] J. F. Hartwig, *Synlett* **1997**, 329.
[16] S. L. Buchwald, *Top. Curr. Chem.* **2001**, *219*, 131.
[17] P. Zacharias, M. C. Gather, M. Rojahn, O. Nuyken, K. Meerholz, *Angew. Chem. Int. Ed.* **2007**, *46*, 4388.
[18] U. Wolf, S. Barth, H. Bassler, *Appl. Phys. Lett.* **1999**, *75*, 2035.
[19] M. K. Mathai, V. E. Choong, S. A. Choulis, B. Krummacher, F. So, *Appl. Phys. Lett.* **2006**, *88*, 243512.
[20] X. H. Yang, F. Jaiser, S. Klinger, D. Neher, *Appl. Phys. Lett.* **2006**, *88*, 3.
[21] P. Piromreun, H. Oh, Y. L. Shen, G. G. Malliaras, J. C. Scott, P. J. Brock, *Appl. Phys. Lett.* **2000**, *77*, 2403.
[22] M. Y. Chan, S. L. Lai, M. K. Fung, C. S. Lee, S. T. Lee, *Chem. Phys. Lett.* **2003**, *374*, 215.
[23] M. Vanderauweraer, F. C. Deschryver, P. M. Borsenberger, H. Bassler, *Adv. Mater.* **1994**, *6*, 199.
[24] K. L. Tong, S. K. So, H. F. Ng, L. M. Leung, M. Y. Yeung, C. F. Lo, *Synth. Met.* **2004**, *147*, 199.
[25] G. G. Malliaras, J. C. Scott, *J. Appl. Phys.* **1998**, *83*, 5399.
[26] Z. X. Wu, L. D. Wang, G. T. Lei, Y. Qiu, *J. Appl. Phys.* **2005**, *97*, 103105.
[27] M. Flammich, M. C. Gather, N. Danz, D. Michaelis, K. Meerholz, *Appl. Phys. Lett.* **2009**, *95*, 263306.
[28] S. L. M. van Mensfoort, M. Carvelli, M. Megens, D. Wehenkel, M. Bartyzel, H. Greiner, R. A. J. Janssen, R. Coehoorn, *Nat. Photonics* **2010**, *4*, 329.